



## OPEN ACCESS

## EDITED BY

Chang-Bo Zheng,  
Kunming Medical University, China

## REVIEWED BY

Rakesh Kumar,  
Washington University in St. Louis,  
United States  
Peng Zhang,  
Institute of ENT and Shenzhen Key Laboratory  
of ENT, China

## \*CORRESPONDENCE

Ji-Jie Pang  
✉ jipang@bcm.edu

RECEIVED 17 July 2024

ACCEPTED 25 September 2024

PUBLISHED 13 November 2024

## CITATION

Pang VY, Yang Z, Wu SM and Pang J-J (2024)  
The co-expression of the depolarizing and  
hyperpolarizing mechanosensitive ion  
channels in mammalian retinal neurons.  
*Front. Med.* 11:1463898.  
doi: 10.3389/fmed.2024.1463898

## COPYRIGHT

© 2024 Pang, Yang, Wu and Pang. This is an  
open-access article distributed under the  
terms of the [Creative Commons Attribution  
License \(CC BY\)](https://creativecommons.org/licenses/by/4.0/). The use, distribution or  
reproduction in other forums is permitted,  
provided the original author(s) and the  
copyright owner(s) are credited and that the  
original publication in this journal is cited, in  
accordance with accepted academic  
practice. No use, distribution or reproduction  
is permitted which does not comply with  
these terms.

# The co-expression of the depolarizing and hyperpolarizing mechanosensitive ion channels in mammalian retinal neurons

Vivian Y. Pang, Zhuo Yang, Samuel M. Wu and Ji-Jie Pang\*

Department of Ophthalmology, Baylor College of Medicine, Houston, TX, United States

**Introduction:** The elevation of the intraocular and extraocular pressures is associated with various visual conditions, including glaucoma and traumatic retinal injury. The retina expresses mechanosensitive channels (MSCs), but the role of MSCs in retinal physiology and pathologies has been unclear.

**Methods:** Using immunocytochemistry, confocal microscopy, and patch-clamp recording techniques, we studied the co-expression of K<sup>+</sup>-permeable (K-MSCs) TRAAK and big potassium channel BK with the epithelial sodium channel ENaC and transient receptor potential channel vanilloid TRPV4 and TRPV2 favorably permeable to Ca<sup>2+</sup> than Na<sup>+</sup> (together named N-MSCs), and TRPV4 activity in the mouse retina.

**Results:** TRAAK immunoreactivity (IR) was mainly located in Müller cells. Photoreceptor outer segments (OSs) expressed BK and ENaC $\alpha$  intensively and TRAAK, TRPV2, and TRPV4 weakly. Somas and axons of retinal ganglion cells (RGCs) retrograde-identified clearly expressed ENaC $\alpha$ , TRPV4, and TRPV2 but lacked TRAAK and BK. Rod bipolar cells (RBCs) showed TRPV4-IR in somas and BK-IR in axonal globules. Horizontal cells were BK-negative, and some cone BCs lacked TRPV4-IR. TRPV4 agonist depolarized RGCs, enhanced spontaneous spikes and excitatory postsynaptic currents, reduced the visual signal reliability ( $VSR = 1 - \text{noise}/\text{signal}$ ) by ~50%, and resulted in ATP crisis, which could inactivate voltage-gated sodium channels in RGCs.

**Conclusion:** Individual neurons co-express hyperpolarizing K-MSCs with depolarizing N-MSCs to counterbalance the pressure-induced excitation, and the level of K-MSCs relative to N-MSCs ( $R_{K/N}$  ratio) is balanced in the outer retina but low in RGCs, bringing out novel determinants for the pressure vulnerability of retinal neurons and new targets for clinical interventions.

## KEYWORDS

TRAAK, BK, TRPV2, TRPV4, ENaC, immunocytochemistry, confocal microscopy, whole-cell patch-clamp

## Introduction

Retinal neurons are vulnerable to pressure stresses in glaucoma (1, 2), traumatic retinal injury (TRI) (3–6), and other conditions (7), and all eukaryocytes express mechanosensitive ion channels (MSCs) to cope with changes in pressure, osmolarity, temperature, shape, and volume (8–10). Multiple types of MSCs are present in retinal neurons, but their role has been unclear.

MSCs vary by structure, ion permeability and selectivity, modulator, and other characteristics. Some MSCs may mediate membrane depolarization, such as Na<sup>+</sup>/Ca<sup>2+</sup>-permeable transient receptor potential channel vanilloid (TRPVs) and Na<sup>+</sup>-permeable epithelial sodium channel (ENaC, SCNN1), and TRPV activation may lead to neuronal excitotoxicity (11–15) and involves the injury to retinal ganglion cells (RGCs) in glaucoma models (16–18). However, not all MSCs mediate depolarizing Ca<sup>2+</sup> or Na<sup>+</sup> currents. In this report, we classified MSCs into two categories based on their permeability and effects on resting membrane potential: the hyperpolarizing K-MSCs permeable to K<sup>+</sup> and the depolarizing N-MSCs selective for Na<sup>+</sup> or nonselective for cations, proposing a potential neuroprotective role of K-MSCs.

Vertebrate retinal rods and the outer plexiform layer (OPL) express N-MSCs like TRPV1 (19), TRPV2 (20–22), and TRPV4 (22, 23), as well as K-MSCs like the big potassium channel (24–26) (BK, also known as the calcium-and voltage-gated large conductance potassium channel, Maxi-K, KCNMA1, Slo1, Kca1.1, and stretch-activated potassium channels) and the two-pore domain K<sup>+</sup> channel (K2P) TRAAK (22, 27) and TREK1 (28). The K<sup>+</sup> channels give rise to leak (also called background) K<sup>+</sup> currents to stabilize the negative resting membrane potential and counterbalance membrane depolarization [reviewed by (9, 29)]. BK and TRAAK are gated primarily by membrane tension (10, 30–34).

TRPs belong to a superfamily of nonselective cation channels with a higher permeability to Ca<sup>+</sup> than Na<sup>+</sup>. TRPV1, TRPV2, and TRPV4 may open upon pressure (35), membrane stretch (36), hypotonicity, or fluid flow (37–44), and the expression has been reported in mammalian retinal ganglion cell layer (GCL) (16–18), inner nuclear layer (INL) (20, 45), plexiform layers (15, 17, 18), and bipolar cells (15) in the mouse, rat, cat, and primate retina [reviewed by (46)]. The GCL and INL also express TREK and TRAAK in the mouse retina (27, 28).

MSCs like TRPV2, TRPV4 (37–44), BK, TRAAK (10, 30–34), and ENaC (8) have been established as mechano-gated channels, which are directly gated by force and opened by membrane stretch and pressure. Pioneering studies on retinal mechanical response started from TRPV4 (17) and TRPV1 (14, 16). In these studies, hypotonicity, static pressure, and channel agonists evoked action potentials and calcium currents in mammalian RGCs. The channel opening was associated with RGC apoptosis (14, 16, 17), and TRPV4 antagonists have showed neuroprotective effects on RGC survival *in vitro* (18) and in a rat glaucoma model (47). Our team has recently reported pressure-evoked cation currents in retinal neurons. In primate bipolar cells (BC) (15), dynamic pressure stimuli opened a cation conductance reversed around ~0 mV, which was consistent with the expression of TRPV4. Similarly, in vertebrate retinal rods and cones, dynamic pressure stimuli evoked three membrane currents, which reversed at ~–80 mV or ~0 mV, aligning with the expression of K-MSCs and TRPVs (22). Moreover, a most recent study from our laboratory has observed significant interference of TRPV4 on light responses of photoreceptors and BCs in living mice *in vivo* (23). Functional studies aligning with morphological and genetic observations have generally established the mechanical responsiveness of retinal neurons.

K-MSCs and N-MSCs are responsive to similar mechanical stimuli, but they mediate currents of opposite polarities given the distinctive reversal potential of ~–80 mV and ≥0 mV, respectively [reviewed by (46)]. Studies usually focus on the activity or location of individual MSCs but rarely assess the co-expression of multiple MSCs,

their relative expression levels, and their combined effects in individual neurons, including retinal neurons (11, 15, 16, 48). Pressure stress is associated with various visual disorders (7, 49–51), but the consequence of pressure-induced activation of retinal MSCs has been unclear.

We investigated the co-presence of several K-MSCs and N-MSCs and the activities of TRPV4 in retinal ganglion cells (RGCs) in the mammalian retina with immunocytochemistry, confocal microscopy, and whole-cell patch-clamp techniques. Our data demonstrated the co-expression of K- and N-MSCs in retinal neurons and TRPV4-mediated RGC dysfunction. The results further suggest that the balance between K-MSCs and N-MSCs, i.e., R<sub>K/N</sub> ratio, is a core mechanism of cellular mechano-homeostasis and a novel determinant for the pressure vulnerability of individual neurons.

## Methods

### Preparations

All procedures were carried out in strict accordance with the Guide for the Care and Use of Laboratory Animals of the National Institutes of Health, ARVO Statement for the Use of Animals in Ophthalmic and Vision Research, and related regulations of the Institutional Animal Care and Use Committee. The animals were 3–7-month-old male and female C57BL/6J mice purchased from Jackson Laboratory (Bar Harbor, ME, USA). Chemicals were purchased primarily from Sigma-Aldrich (St. Louis, MO, USA) and Tocris Bioscience (Bristol, United Kingdom) except otherwise specified.

### Patch-clamp recording of retinal neurons

Animals were dark-adapted for 1–2 h before recording, and all related procedures were performed under infrared illumination. RGCs were recorded from living whole-mount retinas under the loose patch, voltage-clamp, or current clamp mode. The dual-cell patch-clamp recording used MultiClamp 700A or 700 B amplifiers connected to DigiData 1322a interfaces and operated by pClamp software (Axon Instruments, Foster City, CA, USA). Two EPC10 quadruplet amplifiers with digitizers (HEKA instrument, Holliston, MA, USA) provided eight independent channels, which enabled us to record eight cells simultaneously under either voltage- or current-clamp mode. The recording was performed under infrared illumination (>750 nm) or dim red light and monitored by a Nano video camera (Stemmer Imaging AG, Puchheim, Germany). The novel technology has been recently applied to retinal study for the first time by Pang and colleagues (22, 52, 53).

Electrodes were filled with an internal solution containing 0.1–0.5% Lucifer yellow (LY) and/or 2% neurobiotin (NB) with pH adjusted to 7.3 (54–57). Patch pipettes had 5–8 MΩ tip resistance when filled with an internal solution containing 112 mM Cs-methanesulfonate, 12 mM CsCl, 5 mM EGTA, 0.5 mM CaCl<sub>2</sub>, 4 mM ATP, 0.3 mM GTP, and 10 mM Tris, adjusted to pH 7.3 with CsOH. For current-clamp and some voltage-clamp recordings, the pipettes were filled with internal solutions containing 112 mM K-gluconate, 10 mM KCl, 10 mM EGTA, 10 mM HEPES, 0.5 mM CaCl<sub>2</sub>, 1 mM MgCl<sub>2</sub>, 4 mM Na<sub>2</sub>-ATP, and 0.3 mM Na<sub>3</sub>-GTP, adjusted to pH 7.3 by KOH. The internal solution and the external normal Ringer's solution yield an E<sub>Cl</sub> of –59 mV at room temperature.

Recorded cells were visualized by LY and/or NB fluorescence with a confocal microscope (LSM 800, Carl Zeiss, Germany).

## Light stimulation

A photostimulator delivered light spots of a diameter of 600–1,200  $\mu\text{m}$  and 500 nm wavelength ( $\lambda_{\text{max}} = 500 \text{ nm}$ , full width-half max 10 nm) at various intensities ( $-10$  to  $-1 \log I$ ) to stimulate the retina via the epi-illuminator of the microscope (55, 56, 58). The intensity of unattenuated [ $0$  in log unit ( $\log I$ )] 500 nm light from a halogen light source was  $4.4 \times 10^5$  photons.  $\mu\text{m}^{-2} \text{ sec}^{-1}$ . An LED emitting 505 nm light of the unattenuated intensity of  $4 \times 10^3$  photons.  $\mu\text{m}^{-2} \text{ sec}^{-1}$  will be used for multi-cell patch-clamp recording, delivering light spots of 700–1,200  $\mu\text{m}$  in diameter.

## Immunocytochemistry and retrograde labeling of RGCs

Double- and triple-immuno-labeling followed the published experimental protocols (15, 55, 59–62). All fixed retinas were blocked with 10% donkey serum (Jackson ImmunoResearch, West Grove, PA, USA) in TBS [D-PBS with 0.5% Triton X-100 (Sigma-Aldrich) and 0.1% Na<sub>3</sub>N (Sigma-Aldrich)] for 2 h at room temperature or at 4°C overnight to reduce nonspecific labeling. A vibratome (Pelco 102, 1000 Plus; Ted Pella, Inc., Redding, CA, USA) was used to prepare retinal slices. Whole retinas were imbedded in low gel-point agarose (Sigma-Aldrich) and trimmed into a  $10 \times 10 \times 10 \text{ mm}^3$  block. The block was glued onto a specimen chamber mounted on the vibratome and subsequently cut into 40- $\mu\text{m}$  thick vertical sections in PBS solution. Whole retinas and free-floating sections were incubated in primary antibodies in the presence of 3% donkey serum-TBS for 3–5 days at 4°C. Controls were also processed without primary antibodies. Following several rinses, the slices and whole retinas were then transferred into Cy3-, Cy5-, or Alexa Fluor 488-conjugated streptavidin (1:200, Jackson ImmunoResearch), with Cy3- and/or Cy5-conjugated secondary antibodies (1:200, Jackson ImmunoResearch) and/or Alexa Fluor 488-conjugated secondary antibodies (1:200; Molecular Probes, Eugene, OR), in 3% normal donkey serum-TBS solution at 4°C overnight. A nuclear dye, TO-PRO-3 (0.5 mL/mL, Molecular Probes, Eugene, Oregon, USA) was used with the secondary antibody to visualize the nuclei in the retina. After extensive rinsing, retinal preparations were cover-slipped.

RGCs were identified with a double-retrograde labeling technique previously established by Pang and colleagues (60, 61). Briefly, eyeballs of dark-adapted animals were enucleated under the illumination of dim red light. The nerve stump of the freshly dissected eyeball was dipped into a small drop (3  $\mu\text{L}$ ) of 3% Lucifer yellow (Sigma) and/or 8% neurobiotin (NB, Vector Laboratories, CA) in the internal solution (61) for 20 min. Then, the eyeball was thoroughly rinsed with the oxygenated Ames medium (Sigma) to remove the extra dye and dissected under infrared illumination. The dark-adapted eyecup with intact retina and sclera tissue was transferred into fresh oxygenated Ames medium and kept at room temperature for 40 min under a 10 min-dark/10 min-light cycle. Subsequently, the whole retina was isolated from the sclera, fixed in darkness for 30–45 min at room temperature, and visualized with Cy3-, Cy5-, or Alexa Fluor 488-conjugated streptavidin (1,200, Jackson

ImmunoResearch). The technique brightly labeled the entire population of RGCs in the mouse retina (60, 61).

## Antibodies and markers

Antibodies were summarized in Table 1. Polyclonal rabbit anti-TRPV4 (LS-C135, 1: 200; LS-A8583 1:200 and LS-C94498 1: 100) was purchased from LifeSpan Biosciences, Inc. (Seattle, WA, USA). LS-C94498 was raised against a synthetic peptide from the cytoplasmic domain (aa100-150) of mouse TRPV4 conjugated to an immunogenic carrier protein. LS-A8583 targets a synthetic 20-amino acid peptide from the internal region of human TRPV4, and LS-C135 was raised against rat TRPV4 (Q9ERZ8, aa853-871, peptide immunogen sequence: CDGHQQGYAPKWRAEDAPL). LS-C135 provided the best signal-to-noise ratio in the primate retina (15). The specificity of LS-A8583 (17), LS-C94498 (17), and LS-C135 (15, 23) for labeling retinal TRPV4 were confirmed in TRPV4 transgenic mice.

Purified polyclonal goat-anti TRAAK was purchased from Santa Cruz (sc-11324, goat, 1: 100). It was raised against a peptide mapping at the C-terminus of TRAAK of human origin, which identified a single band at  $\sim 47 \text{ kDa}$  in IMR-32 and Y79 whole cell lysates, matching TRAAK (63). TRPV2 antibodies included a rabbit anti-rat (1: 200, PC241, Calbiochem, San Diego, CA, USA) and a goat anti-mouse (LSbio, Lynnwood, WA, USA) polyclonal antibody, and the antigens were a synthetic peptide aa 744–761 of rat TRPV2 (44, 64) and a peptide aa743-756 of mouse TRPV2 with the sequence C-SEEDHLPLQLQSH. Monoclonal mouse anti-BK was purchased from MilliporeSigma (1: 500, MABN70, anti-Slo1, clone L6/60, pore-forming alpha unit), and it primarily identifies a single band  $\sim 100 \text{ kDa}$  close to MW 100–130 kDa of BK (65, 66). Polyclonal rabbit anti-ENaC $\alpha$  was from Abcam (1, 200, Cambridge, MA, USA) (67–69), which identified a single band at  $\sim 75 \text{ kDa}$  in human platelet lysates, matching ENaC $\alpha$ .

Protein Kinase-C alpha (PKC $\alpha$ ) is a classic marker for rod BCs (55, 70, 71). The anti-PKC $\alpha$  antibody from Sigma (P4334, 1: 1000, rabbit, polyclonal) was tested in immunoblotting with rat brain extract, and it recognized a heavy band at  $\sim 76 \text{ kDa}$  and a very weak band at 40 kDa, while the predicted molecular weight of the PKC $\alpha$  was 76–93 kDa. The staining was specifically inhibited by PKC $\alpha$  immunizing peptide (659–672). The monoclonal anti-PKC $\alpha$  antibody from BD transduction [610107, Clone 3/PKC $\alpha$  (RUO), 1: 200, mouse] identified a single band at 82 kDa from a rat cerebrum lysate. Two calbindin D-28k antibodies were used to identify horizontal cells (72), one of which was a rabbit polyclonal antibody raised against the recombinant rat calbindin D-28 K (CB) protein purchased from Swant (Marly 1, Switzerland) (CB38, 1: 1000) (73, 74), and the other was a mouse monoclonal antibody purchased from Sigma and produced with the bovine kidney calbindin-D (C9848, clone CB955, 1: 200) (73, 74). Monoclonal mouse anti-glutamine synthetase (GS) (1: 1000, clone 6, BD Transduction Laboratories, Palo Alto, CA) was used to identify Müller cells (60). The antibody was raised against the human glutamine synthetase aa 1–373 and recognized a band at  $\sim 45 \text{ kDa}$ , consistent with the predicted molecular weight of GS. Other primary antibodies included in this study have also been used in previous reports, including polyclonal guinea pig anti-GABA (1:1000, AB175; Chemicon, Temecula, CA, USA) (75) and rat anti-glycine antiserum

TABLE 1 Antibodies.

Name	Source, Catalog number, Host, dilution	Antigen	Specificity	References
TRPV4	Lifespan bioscience, LS-C135, rabbit, 1: 500	Q9ERZ8, aa853-871 of rat TRPV4	Confirmed on mutant mice	(15, 23)
TRPV2 IgG	Calbiochem, PC421, rabbit, 1: 200	Synthetic peptide aa 744–761 of rat TRPV2	Identified a single band at ~90 kDa of the full length TRPV2	(44, 64)
TRPV2	Lifespan bioscience, LS-C112764, goat, 1: 100	Synthetic peptide aa743–756 of mouse TRPV2	Identified a single band at ~100 kDa in rat brain lysates close to MW of 86 kDa of TRPV2	(22)
TRAAK	Santa Cruz, sc-11324, goat, 1: 100	A peptide mapping at the C-terminus of TRAAK of human origin.	Identified a single band at ~47 kDa, matching TRAAK.	(7, 63)
BK (slo 1) monoclonal	Millipore, MABN70, mouse, 1: 500	Recombinant protein corresponding to the S9-S10 segment of mouse slo 1.	Identified a single band at ~100 kDa in rat brain lysates, matching MW 100–130 kDa of BK.	(65, 66)
ENaC $\alpha$	Abcam, ab65710, rabbit, 1: 200	Amiloride-sensitive ENaC $\alpha$ (human)	Identify a single band at 75 kDa in human platelet lysates, matching ENaC $\alpha$ .	(67–69)
ENaC $\beta$	Abcam, ab21795, mouse, 1: 100	aa 541–640 of Human ENaC $\beta$ .	Identified two bands in protein extract of <i>E. coli</i> and did not respond to a negative control fusion protein.	
PKC $\alpha$ antiserum	Sigma, P4334, rabbit, 1: 1 K	Synthetic peptide corresponding to aa from the C-terminal V5 region of rat PKC $\alpha$ conjugated to KLH.	Recognized a heavy band at ~76 kDa and a very weak band at 40 kDa in rat brain extract, in line with MW 76–93 kDa of PKC $\alpha$ .	(55, 70, 71)
PKC $\alpha$ monoclonal	BD bioscience, 610107, mouse, 1: 200	Human PKC $\alpha$ aa270-427	a single band at 82 kDa close to MW 76–93 kDa of PKC $\alpha$ .	(55, 70, 71)
Glutamine synthetase (GS) monoclonal	BD Transduction, 610517, 610518, clone 6, mouse, 1: 1 K	human glutamine synthetase aa 1–373	Recognized a band at ~45 kDa, consistent with the predicted MW of GS.	(60)
Calbindin D-28 K	Swant, CB38, rabbit, 1: 1 K	recombinant rat calbindin D-28 K	Immunoblot of brain homogenate of the mouse, rat, guinea pig, rabbit, macaca, zebrafish, and chicken detects only a single band at 28 kDa. Negative results in knockout mice.	(73, 74)
Calbindin-D-28 K, monoclonal	Sigma, C9848, clone CB955, mouse, 1: 200	bovine kidney calbindin-D, 28 kDa	Does not react with other members of the EF-hand family	(73, 74)

(1:1000, a generous gift from Dr. David Pow, University of Queensland, Brisbane, QLD, Australia) (76). The specificity of these primary antibodies has been demonstrated in previous studies, and their staining patterns in our results were similar to the reports. Controls were also processed with blocking peptides or without primary antibodies. All controls did not show positive results.

## Data analysis

We used confocal microscopes (510 and LSM 800, Carl Zeiss, Germany) for morphological observation. Pixel intensities of MSC

immunoreactivities were analyzed in different retinal layers with the confocal (Zen Blue, Zeiss), Sigma plot (v12 and 15), and Excel software and fitted to an exponential function (15).

$$f(I) = a * \exp\{-0.5 * [\frac{(I - I_0)}{b}]^2\} \quad (1)$$

where  $a$  is the pixel count at the distribution peak,  $I$  is the pixel intensity, and  $I_0$  is  $I$  at the distribution peak, and  $b$  is a slope/width factor. The ATP consumed by RGCs for maintaining resting membrane potential (ATP<sub>RP</sub>, molecules/s) was calculated by the previously established equation (95)

$$ATP_{RP} = \frac{N_A}{F} * \frac{(V_{Na} - RP) * (RP - V_K)}{R_m * (RP + 2 * V_{Na} - 3 * V_K)} \quad (2)$$

where  $V_{Na}$  (+50 mV) and  $V_K$  (-100 mV) are Nernst potentials for  $Na^+$  and  $K^+$ ,  $N_A/F = 6.2 \times 10^{18}$ , and  $N_A$  and  $F$  are the Avogadro and Faraday constant, respectively. Data were further analyzed by Sigmaplot (v12 and v15, Systat, Point Richmond, CA, USA), Clampfit (v10.3 and v9.2, Axon Instruments, Foster City, CA, USA), Matlab, and Microsoft Excel for statistical significance. The  $\alpha$  level to reject the null hypothesis is 0.05.

## Results

### BK expression in retinal layers

BK was the most heavily expressed in the outer segment layer (OSL) (Figures 1C,D), and weaker immunoreactivity (IR) was also present in the OPL, IPL, some somas in the INL and GCL (Figure 1A), and large globules of axon terminals of rod bipolar cells (RBCs) (Figure 1B and the inset of Figure 1A). Horizontal cells identified by calbindin D-28 K antibody were nearly negative for BK (Figure 1E). The peak intensity of the fitting curve of the pixel histogram (Equation 1) showed that the relative intensity of BK-IR was in the

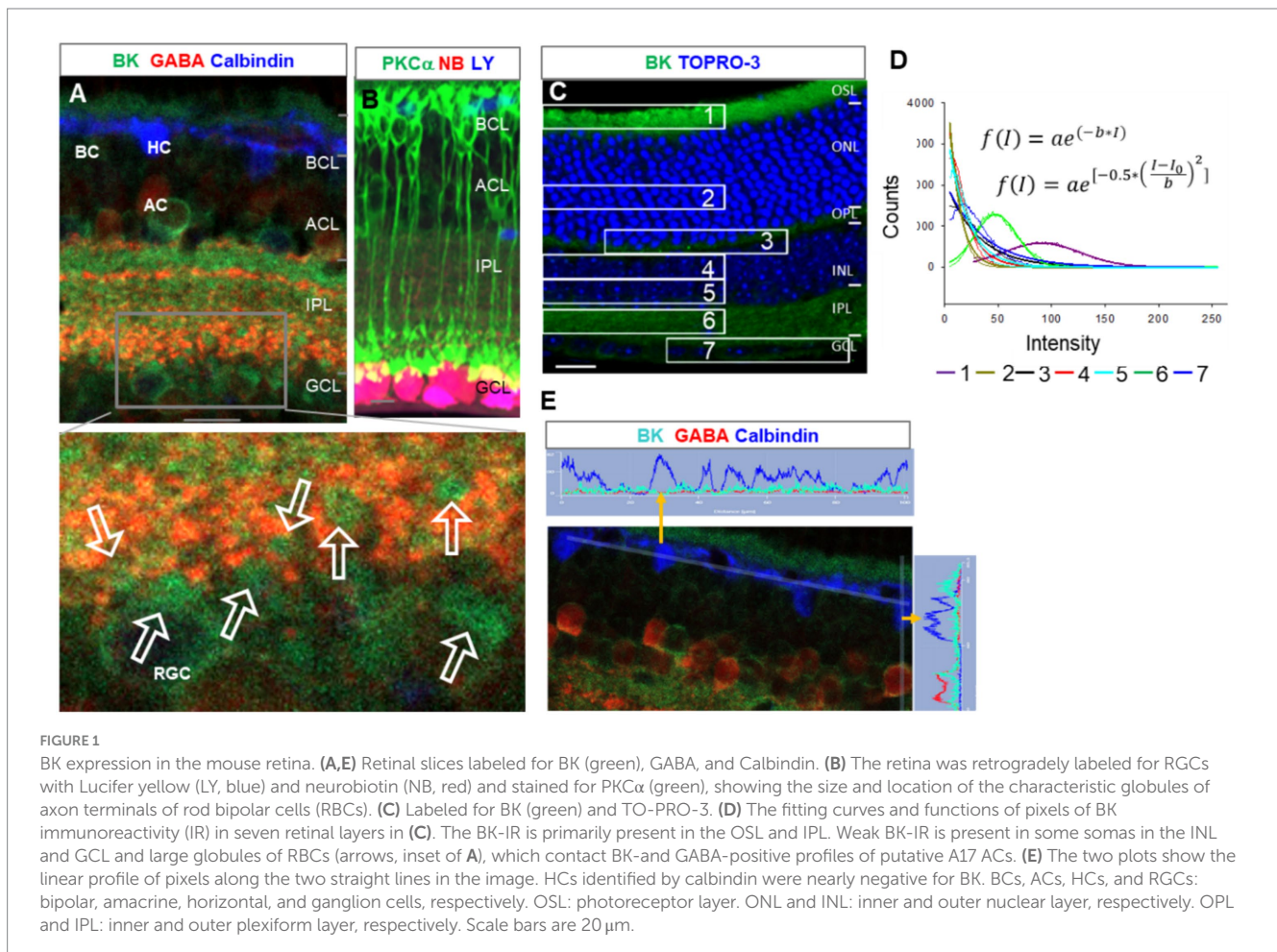
order of  $OSL > IPL \approx RBC \text{ axons} > OPL \approx GCL/INL$ . BK-IR identified some GABAergic somas of ACs and dendrites of putative A17 ACs that contacted the axon terminal of  $PKC\alpha$ -positive RBCs (Figure 1A).

### TRAAK expression in retinal layers

In triple-labeled retinal slices, TRAAK (Figure 2A<sub>1</sub>) was heavily expressed in Müller cells, including the somas in the middle of the INL, end feet in the GCL, and descending processes passing the INL and IPL. The OSL and OPL were weakly labeled. The relative intensity of TRAAK-IR was in the order of  $Müller \text{ cells} > OSL \approx OPL$ . In Figures 2A,B, RGCs were retrogradely identified, and RGC somas were nearly negative for TRAAK.

### The co-expression of depolarizing TRPV4 with the hyperpolarizing BK and TRAAK

In labeled retinal slices, TRPV4-IR was more intensive in retrograde-labeled RGC somas in the GCL (Figures 2A<sub>2</sub>,B). It was weaker in other layers and nearly absent in the inner segment layer (ISL) of photoreceptors. TRPV4-IR was mostly diminished in homozygotes with TRPV4 expression suppressed ( $TRPV4^{-/-}$  mice), demonstrating the specificity of the antibody (Figure 2D).



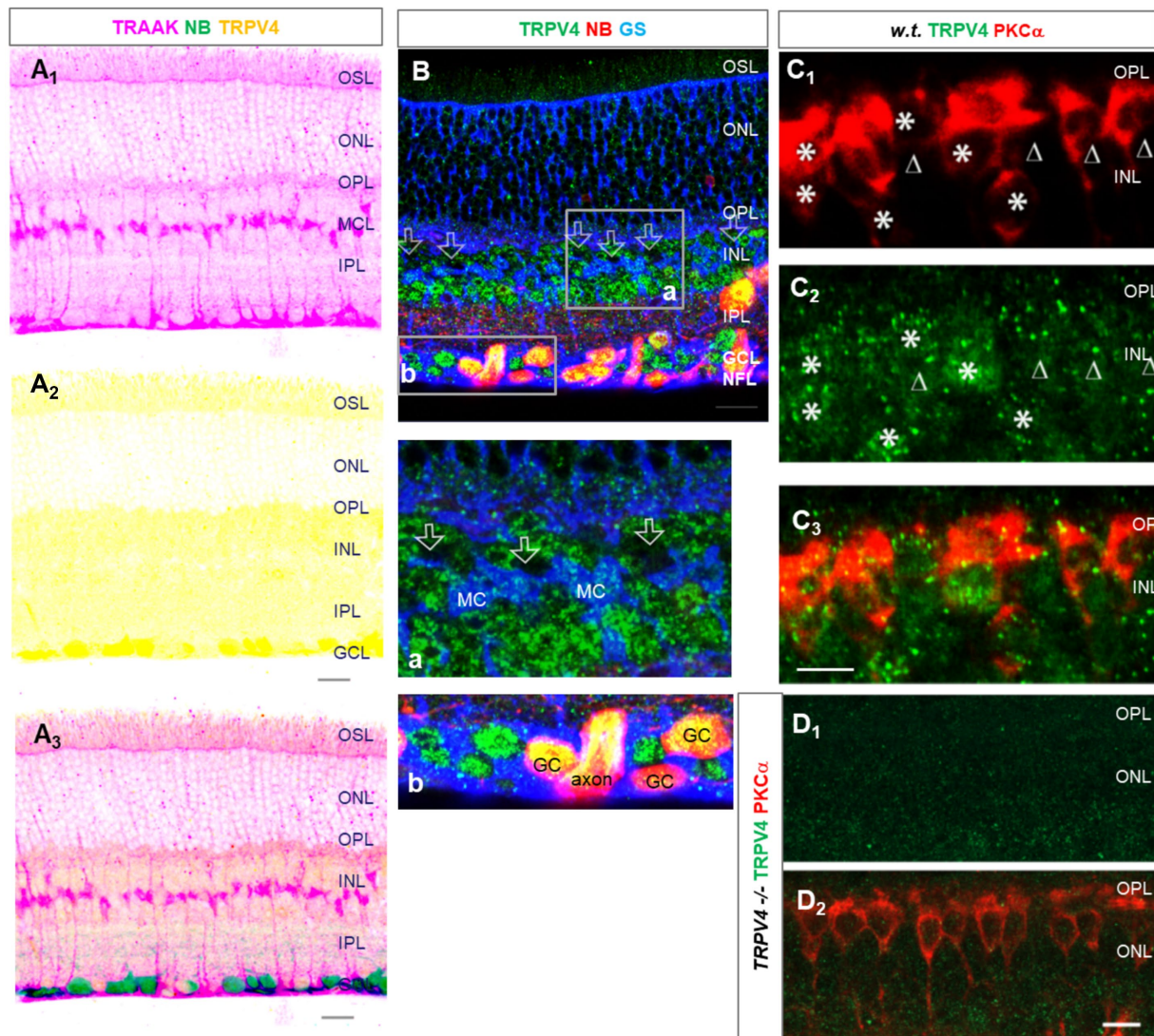


FIGURE 2

The expression of TRAAK and TRPV4 in the mouse retina. (A,B) Retinal slices were retrogradely labeled for ganglion cells (GCs) by neurobiotin (NB) and stained for TRPV4 (green) and TRAAK (A, pink) or glutamine synthetase (GS, blue, B). TRPV4 signals are heavier in the GCL. (A) The image was inverted and displaced on a white background. TRAAK is heavily expressed in Müller cells and weakly expressed in OSL and OPL. (B) Axons and somas of GCs are brightly positive for TRPV4. TRPV4 is present in Müller cells (MC). Some somas of putative cone BCs in the second soma row of the INL contain no TRPV4 signals (open arrow, inset b). (C,D) Retinal slices from wild-type (w.t.) and TRPV4 transgenic mice (TRPV4<sup>-/-</sup>) were labeled for TRPV4 (green) and PKC $\alpha$  (red). (C) Some TRPV4 puncta are present in rod BCs (asterisks) and cone BCs (triangles). (D) TRPV4 signal is nearly absent in TRPV4 transgenic mice. OSL: outer segment layer; ISL: inner segment layer; OPL: outer plexiform layer; INL: inner nuclear layer; BCL: bipolar cell layer; ACL: amacrine cell layer; IPL: inner plexiform layer; GCL: ganglion cell layer; NFL: nerve fiber layer. The scale bar is 5  $\mu$ m for C and 20  $\mu$ m for others.

TRPV4-IR was also present in PKC $\alpha$ -identified RBCs (Figure 2C, asterisk), some PKC $\alpha$ -negative cone bipolar cells (Figure 2C, triangle), and GS-identified Müller cells (Figure 2B). Some somas of putative cone bipolar cells were negative for TRPV4 (Figure 2B, inset b). The relative intensity of TRPV4-IR was in the order of  $GCL > OSL \approx OPL \approx IPL \approx INL$ .

The results (Figures 1, 2) together revealed that the OSL expressed BK, TRAAK, and TRPV4; RGCs possessed the highest level of TRPV4 and a low level of BK and lacked TRAAK; INL, IPL, and OPL weakly co-expressed TRPV4 and BK. The higher level of depolarizing TRPV4 in RGCs is consistent with their higher pressure-vulnerability observed in glaucoma (1, 2) and traumatic retinal injury (3–6) compared to other neurons.

## The expression of depolarizing TRPV2 and ENaC in the mouse retina

TRPV2 was expressed primarily in the OPL, IPL, and retrograde-identified RGCs, and TRPV2-IR was weak in the OSL and INL and nearly absent in the ISL. The relative intensity of TRPV2-IR was in the order of  $IPL \approx OPL > GCL > OSL \approx INL$  for wild-type mice. TRPV2-IR was heavier in the GCL and ACL in the congenital glaucoma model DBA/2J (D2) mice, and the relative intensity was in the order of  $GCL \approx ACL > OPL \approx OSL$  (Figure 3).

ENaC $\alpha$  was intensively expressed in photoreceptors, OPL, IPL, and RGC somas and dendrites, and the INL was weakly labeled. The

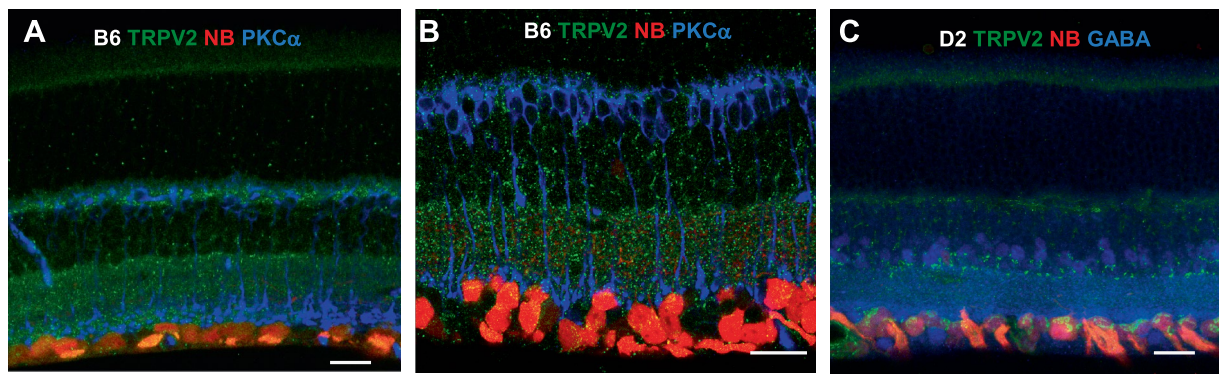


FIGURE 3

TRPV2 expression in mouse retina. RGCs were retrogradely labeled by neurobiotin (NB, red). (A,B) TRPV2 (green) is expressed in the OSL, OPL, IPL, and GCL (A). Some puncta are present in RGCs identified by PKC $\alpha$  immunoreactivity (B, blue). The expression in the ACL and GCL is heavier in DBA/2J mice (D2, a congenital glaucoma model, in C), including amacrine cells labeled for GABA (C, blue). B6: C57BL/6J mice. Scale bars are 20  $\mu$ m.

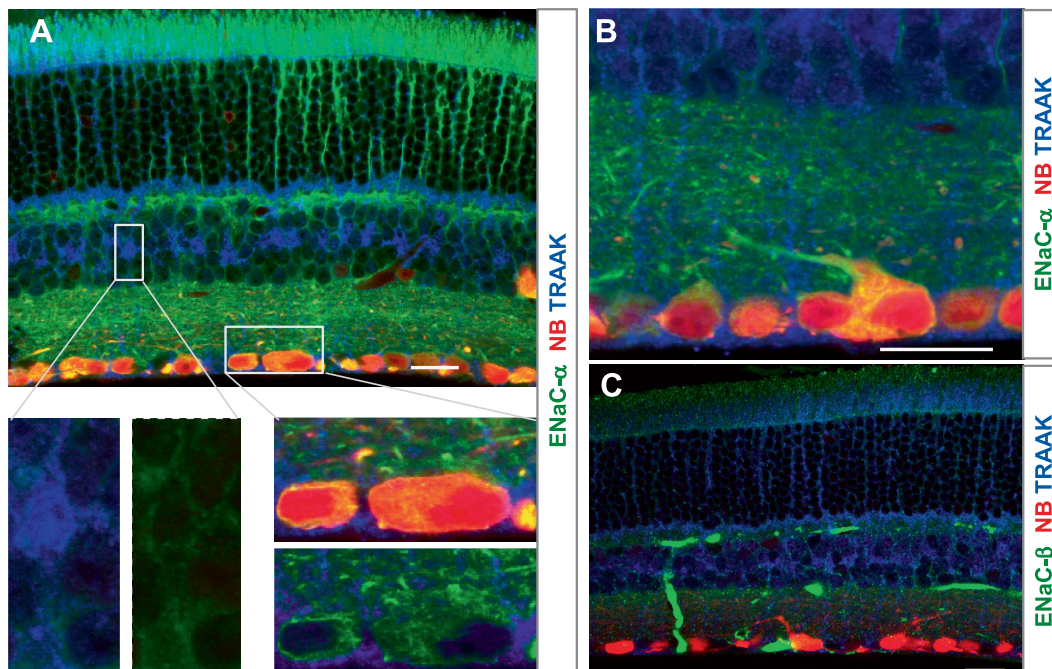


FIGURE 4

The expression of the mechanosensitive ENaC in mouse retina. Retinas were retrogradely labeled for RGCs by NB (red) and stained for TRAAK (blue) and ENaC $\alpha$  (A,B) or ENaC $\beta$  (C) (green). (A,B) ENaC $\alpha$  is intensively expressed in photoreceptors, OPL, IPL, and RGC somas and dendrites, and the INL is weakly labeled. TRAAK is primarily expressed in the soma, process, and end foot of Müller cells and OSL (A–C). (C) ENaC $\beta$  identifies blood vessels and weakly labels the OSL, OPL, and IPL. Scale bars are 20  $\mu$ m.

relative ENaC $\alpha$ -IR was in the order of *photoreceptors*  $\approx$  *GCL*  $\approx$  *OPL*  $\approx$  *IPL*  $>$  *INL* (Figure 4). The ENaC $\beta$  antibody stained blood vessels and weakly labeled the OSL, OPL, and IPL (Figure 4C). The distribution of these depolarizing MSCs was nearly even in the outer and inner retina but favored neurons over Müller cells. In Figures 3, 4, all RGCs were retrogradely identified.

In summary, the relative expression level was in the order of *Müller cells*  $>$  *OSL*  $\approx$  *OPL* for TRAAK, *OSL*  $>$  *IPL*  $\approx$  *RBC axons*  $>$  *OPL*  $\approx$  *GCL*  $\approx$  *INL* for BK, *GCL*  $>$  *OSL*  $\approx$  *OPL*  $\approx$  *IPL*  $\approx$  *INL* for TRPV4, *GCL*  $\approx$  *ACL*  $>$  *OPL*  $\approx$  *OSL* for TRPV2 (in D2 mice), and *GCL*  $\approx$

*photoreceptors*  $\approx$  *OPL*  $\approx$  *IPL*  $>$  *INL* for ENaC $\alpha$ . TRAAK was expressed mainly in Müller cells. Photoreceptors expressed BK and ENaC $\alpha$  intensively and TRAAK, TRPV2, and TRPV4 weakly. RGC somas and axons retrograde-identified clearly expressed ENaC $\alpha$ , TRPV4, and TRPV2 but lacked TRAAK and BK. BCs weakly expressed BK, ENaC $\alpha$ , and TRPV4. Some amacrine cells were positive for BK, ENaC $\alpha$ , and TRPV4. These results indicate a higher ratio of K-MSCs to N-MSCs ( $R_{K/N}$ ) in photoreceptors and interneurons than RGCs, which is consistent with the high pressure-vulnerability of RGCs in glaucoma.

## TRPV4-induced excitation and dysfunction of mouse RGCs

We have previously characterized mouse RGCs by the resting potential, synaptic currents, and firing features (57, 77). Since TRPV4 mediates excitatory cation current, we further study the role of TRPV4 in RGCs with TRPV4 agonists 4 $\alpha$ -Phorbol 12,13-didecanoate (4 $\alpha$ PDD) and GSK101 (GSK, GSK1016790A). The results showed that TRPV4 agonists enhanced the firing rate of spontaneous action potentials (Figures 5A,B) recorded under the loose-patch mode and the frequency and amplitude of the spontaneous and light-evoked excitatory postsynaptic currents (sEPSCs and  $\Delta I_C$ , respectively) (Figures 5D–G) under the voltage-clamp mode in all RGCs. In Figures 5A,B, the ON $\alpha$ RGC generated light-evoked action potentials (APs) with little visual noise, while 4 $\alpha$ PDD induced many spontaneous APs, i.e., visual noises, which were unrelated to the light. Similarly, Figures 5F,G showed that in another ON $\alpha$ RGC, 4 $\alpha$ PDD enhanced the amplitude and frequency of sEPSCs unrelated to the light. We further measured the frequency of light-evoked APs (Signal, S) and light-unrelated APs (Noise, N) in the same RGCs before and after application of drugs. In the presence of the drugs, the visual signal reliability (VSR), calculated by ( $VSR = 1 - N/S$ ) (Figure 5C), was reduced by ~50% ( $p < 0.001$ ) in ON RGCs. Since

the vesicle release from presynaptic terminals primarily determines the frequency of sEPSCs and the postsynaptic mechanism dominates the amplitude of sEPSCs, these data indicate that the TRPV4-induced excitation in RGCs involves TRPV4 in both BCs and RGCs.

Figure 6 showed that activating MSCs with low osmolarity (Osm) and TRPV4 agonists 4 $\alpha$ PDD and GSK101 significantly depolarized membrane potential in all RGCs (Figures 6A,B). 4 $\alpha$ PDD elicited spontaneous firing of APs (Figure 6A) was reversibly blocked by a general TRPV antagonist ruthenium red (RR). TRPV4 induced membrane depolarization and spontaneous firing would need to consume extra ATPs. Thus, we plotted the ATP consumption for maintaining normal resting potential based on Equation 2 (Figure 6D, blue curve). The data showed that TRPV4-induced depolarization raised the ATP consumption to the peak, predicting ATP depletion. We also recorded Na<sup>+</sup> currents ( $I_{Na}$ ) in RGCs mediated by voltage-gated Na<sup>+</sup> channels (NaV) under voltage-clamp conditions by depolarizing RGCs from  $-110$  or  $-70$  mV with a step of 8–20 mV. The evoked responses could not be significantly affected by BC and AC synapses.  $I_{Na}$  was an inward current at the holding potentials of  $\leq 40$  mV and identifiable from potassium, chlorides, and calcium currents by the duration of ~2 ms and the polarity of the spike.  $I_{Na}$  was found to activated at  $\sim -50$  mV ( $n = 5$  cells) and sensitive

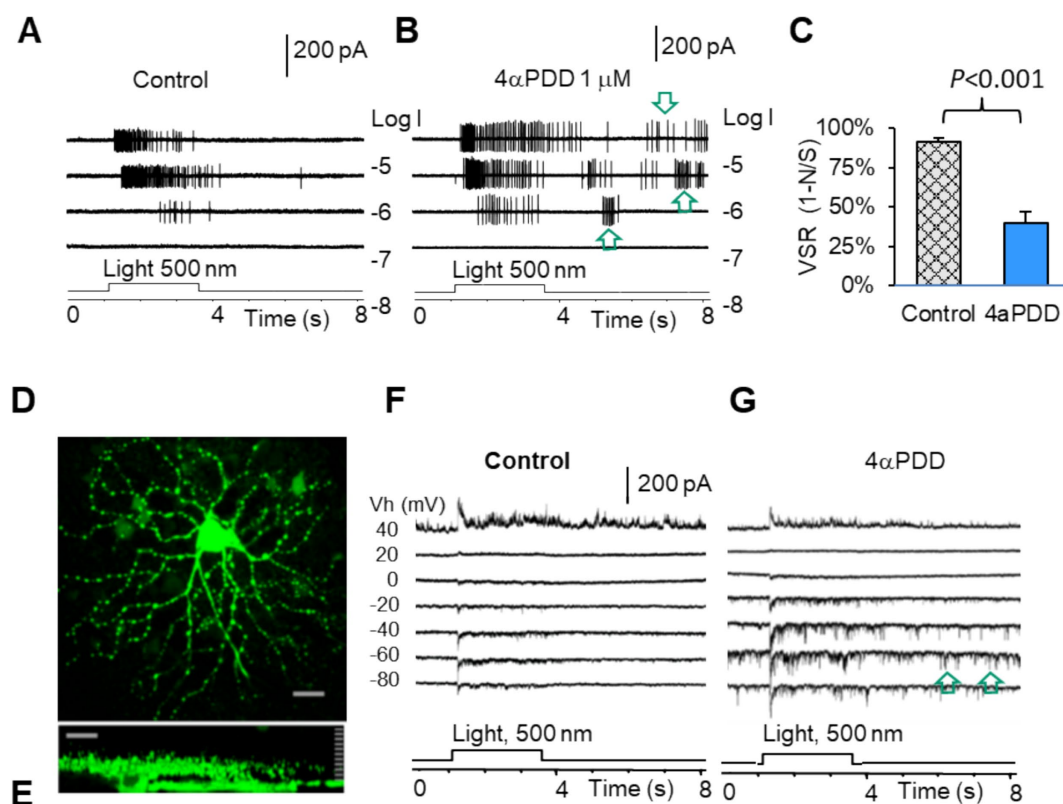


**FIGURE 5** TRPV4 mediates excitatory visual noises and dysfunction of mouse RGCs. RGCs were recorded under loose patch mode (A,B) and whole-cell voltage-clamp mode at various holding potentials (D–G). (A,B,F,G) TRPV4 agonists enhance spontaneous action potentials (A,B, arrow) and the spontaneous postsynaptic currents (arrow) and light-evoked excitatory currents (F,G), reducing the visual signal reliability [ $VSR = 1 - \text{noise (N)}/\text{signal (S)}$ ] by ~50% (C). (D,E) Confocal images of a recorded RGC filled with Lucifer yellow (D: The x-y view; E: The y-z view revealing the dendritic tree and axon of the cell).

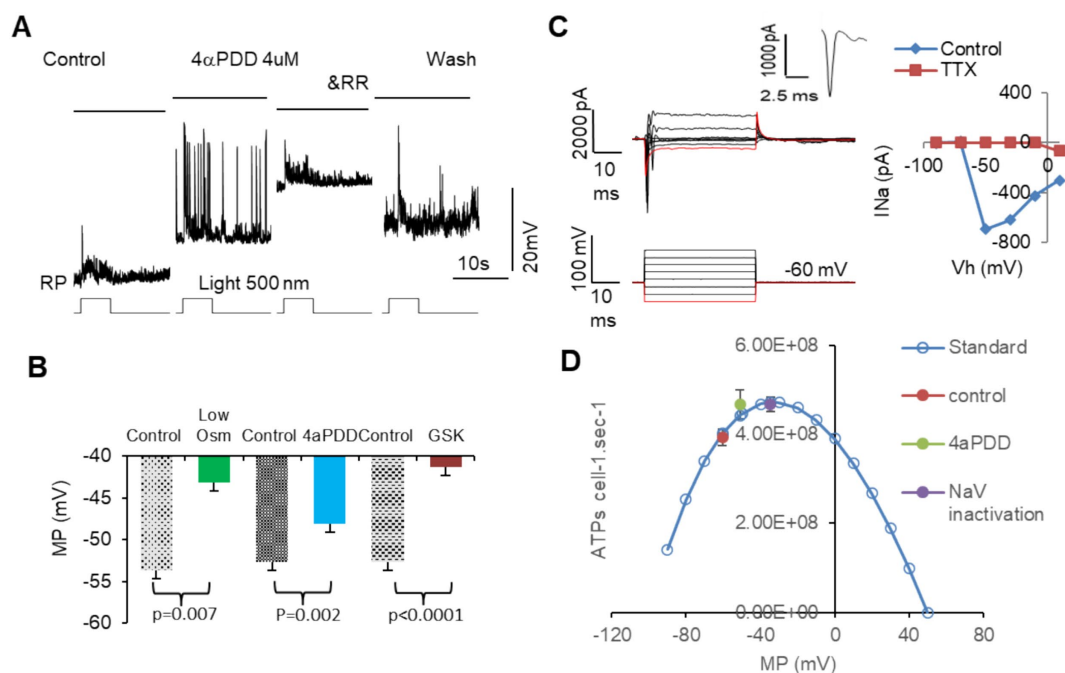


FIGURE 6

The activation of MSCs induces membrane depolarization, ATP depletion, and dysfunction of mouse RGCs. RGCs are recorded under current-clamp (A,B) and voltage-clamp (C) modes. (A,B) Activating MSCs by low osmolarity (Osm) and TRPV4 agonists 4αPDD and GSK101 (GSK) depolarizes MP of RGCs to  $-40$  to  $-50$  mV and elicits spontaneous firing of action potentials (A), which raises the ATP consume close to the peak level and predicts ATP depletion. (C) The threshold of NaVs in mouse RGCs is close to  $-50$  mV and sensitive to TTX. The duration of the sodium current is  $\sim 2$  ms. (D) Blue curve: the standard ATP consumption for RGCs to maintain RP was plotted per Equation 2. TRPV4 agonists raised the ATP consumption to the peak level (green dot) near the inactivation level of half NaVs (purple dot). Vh: holding potential. MP: membrane potential. RP: resting potential. NaV: voltage-gated sodium channel. RR: ruthenium red, nonspecific blocker of TRPs.

to TTX (Figure 6C), consistent with typical NaVs well documented in previous studies (78, 79). The peak of the ATP consumption curve just overlapped with the membrane potential ( $\sim -37$  mV) where half NaVs underwent slow inactivation (purple dot, Figure 6D) (80), and TRPV4 agonists also raised the ATP consumption to the peak level (green dot, Figure 6D), indicating that ATP depletion and RGC malfunction may follow intensive TRPV4 activation.

The results together demonstrated that TRPV4 activation directly induced depolarization and dysfunction of RGCs, and the effect is associated with TRPV4 expressed in BCs and RGCs, expedited inactivation of NaVs in RGCs, and ATP overconsumption.

## Discussion

### Individual retinal neurons co-express several K- and N-MSCs for cellular mechano-electro-homeostasis

The retina expresses multiple MSCs (11, 21, 46), while studies often focus on individual types of MSCs. It has been unclear whether individual retinal neurons co-express multiple MSCs and the significance of such design. The elevation in intra- and extra-ocular

pressure closely involves the pathogenesis of glaucoma and other retinal conditions (1–7), and the question of whether retinal neurons were directly responsive to the mechanical signals had not been addressed until recent years when mechanical responses were revealed from RGCs (14, 17), BCs, and photoreceptors (15, 22). MSCs generate electric currents in retinal neurons upon activation. Since many MSCs, including TRPV4, TRPV2, BK, TRAAK, and ENaCa, are not classic molecules that serve light pathways in the retina, their physiological and pathophysiological role remains to be defined (11, 46, 81–84).

We discovered the co-expression of several MSCs in retinal layers and individual neurons, including N-MSCs that mediate inward cation currents and K-MSCs that carry outward K<sup>+</sup> current at membrane potential levels between  $-80$  and  $0$  mV (46). The morphological data, consistent with functional results obtained from photoreceptors and BCs in the salamander (22) and mammalian retina (15, 23), demonstrates that outer retinal neurons possess several types of MSCs. We postulate that a cell with more MSCs would theoretically possess better mechanical adaptability, and because of the opposite polarity of the electric currents at K- and N-MSCs, a balanced ratio of K- and N-MSCs would better reduce the pressure-induced instantaneous electric disturbance on neuronal signals. Supporting this idea, our data revealed a distinct  $R_{K/N}$  ratio in retinal neurons, and the more

balanced one in the outer retinal neurons well aligns with their lower pressure vulnerability in glaucoma and traumatic retinal injury (1–7). It indicates that the pressure responsiveness of a cell is to be determined by both the level and ratio of K- and N-MSCs, establishing a novel mechanism of cellular mechanical homeostasis in sensory neurons that may provide not only mechano-protection to cellular physical integrity but also electro-protection to neuronal signals by reducing mechanically induced electric noises.

Recent work has also identified the interaction between TRPs and BK in smooth muscles and between TRPV4 and another calcium-activated potassium channel KCa2.3 in the endothelial cells of blood vessels (85–87). BK mediates muscle relaxation, and TRPV4 mediates contraction after the relaxation (86), supporting the notion of the counterbalance between these channels.

## The relative level of hyperpolarizing MSCs and depolarizing MSC is critically associated with neuroprotection and neurodegeneration

RGCs showed higher pressure vulnerability in glaucoma and traumatic retinal injury than other retinal neurons (1–7). Depolarizing N-MSCs such as TRPV4 and TRPV1 can mediate RGC depolarization, spontaneous firing, and cell death (14, 15, 17, 88), and our patch-clamp data was in line with previous reports. More importantly, we used VSR to demonstrate TRPV4-mediated RGC dysfunction, and we further calculated TRPV4-related ATP depletion and the likelihood of inactivating voltage-gated sodium channels (NaVs). Meanwhile, our immunological data confirmed a much higher expression level of depolarizing N-MSCs relative to K-MSCs in RGCs but similar levels of N- and K-MSCs in outer retinal neurons. These results together support the idea that a low  $R_{K/N}$  or a high  $R_{N/K}$  plays a pro-neurodegenerative role in neurons.

The excitotoxic effect of TRPVs previously reported in RGCs has suggested that blockage or removal of TRPVs may be beneficial (14, 15, 17, 18, 88), but whether it would compromise the pressure adaptability of the neurons is still uncertain. ENaC and TRPVs carry cation currents to reverse at  $\geq -0$  mV, while K-MSCs like BK and TRAAK mediate background leak currents to reverse at  $\sim -80$  mV (46). Thus, at the membrane potential (RP) level of  $0 > RP > -80$  mV, K-MSCs would counterbalance N-MSC-induced membrane depolarization. Based on current results, raising  $R_{K/N}$  appears to be a safer strategy to reduce pressure-induced excitotoxicity than solely reducing N-MSCs.

Membrane potential alters the driving force of MSCs and is another factor that modulates currents at MSCs besides  $R_{K/N}$ , while RGCs maintain RPs less depolarized than outer retinal neurons (22, 57, 89–93). Hence, we postulate that RGCs are less protected by K-MSCs and more easily activated by N-MSCs compared to outer retinal neurons, and this mechanism could also contribute to the high vulnerability of RGCs. Our data discovered a low  $R_{K/N}$  in RGCs, suggesting  $R_{K/N}$  as a novel determinant of pressure-induced excitotoxicity and improving  $R_{K/N}$  as a new therapeutic strategy.

## MSCs mediate electric noise, dysfunction, and ATP crisis in RGCs

RGCs express TRPV4 in the mouse (16, 17, 94), porcine (18), and primate retina (15), and TRPV4 agonists excite RGCs (15, 17). Our data are consistent with previous findings. Besides membrane depolarization, we revealed that TRPV4 agonists caused more robust excitatory postsynaptic current ( $EPSC_{TRPV4}$ ) and dramatic reduction of VSR, predicting ATP depletion in RGCs.  $EPSC_{TRPV4}$  may involve TRPV4-IR in both BCs and RGCs.

Using VSR (1-N/S, %), we measured the reliability of the light-evoked action potentials under the disturbance of TRPV4 opening, creating an accurate measure for the dysfunction of individual RGCs. Neurons consume most energy to maintain the normal membrane potential (i.e., the normal electrochemical gradient of ions), as the latter is frequently disrupted by the opening of ion channels on the plasma membrane (95). Cation fluxes via opened ion channels follow and, thus, consume their electrochemical gradients across the membrane. The reduced gradients need ATPase and energy to recover (95). We first explored the relationship between the effect of TRPV4 activation, RP, activities of NaVs, and ATP consumption in RGCs. Our results showed that TRPV4 activation depolarized RGCs to the RP level that would inactivate NaVs (78–80, 96) and maximize ATP consumption. The results further suggest that improving ATP levels should be considered in treating pressure-related visual diseases.

Although currents at K- and N-MSCs are generally mutually compensating because of the opposite polarity, TRPs are known to mediate transient currents (15, 43, 84, 97), and K-MSCs carry leak currents (22, 28, 29). The difference in their kinetics does not allow complete cancellation of the pressure-induced current noise even with a balanced  $R_{K/N}$ . Our data indicates that opening TRPVs in retinal neurons can reduce VSR and increase ATP consumption in RGCs, predicting ATP crisis and pathologies if the pressure stress is persistent. Further studies on MSCs in retinal neurons will likely substantially facilitate the early diagnosis and treatment of pressure-related retinal disorders.

## Data availability statement

The original contributions presented in the study are included in the article/supplementary material, further inquiries can be directed to the corresponding author.

## Ethics statement

The animal study was approved by the Institutional Animal Care and Use Committee (IACUC). The study was conducted in accordance with the local legislation and institutional requirements.

## Author contributions

YYP: Data curation, Writing – original draft, Formal analysis. ZY: Methodology, Writing – original draft, Visualization. SMW: Funding

acquisition, Resources, Writing – original draft. J-JP: Conceptualization, Data curation, Formal analysis, Funding acquisition, Investigation, Methodology, Project administration, Resources, Supervision, Validation, Visualization, Writing – original draft, Writing – review & editing.

## Funding

The author(s) declare financial support was received for the research, authorship, and/or publication of this article. This work was supported by U.S. Army Medical Research Acquisition Activity VR210010 W81XWH2210741 (the major support for salaries and experiments), EY033492, NIH Vision Core (EY 02520) (support for facilities), Retina Research Foundation (Houston) and Research to Prevent Blindness, Inc. (support for environment and some equipment). Opinions, interpretations, conclusions, and recommendations are those of the authors and are not necessarily endorsed by the funders.

## References

- Jonas JB, Aung T, Bourne RR, Bron AM, Ritch R, Panda-Jonas S. Glaucoma. *Lancet*. (2017) 390:2183–93. doi: 10.1016/S0140-6736(17)31469-1
- Quigley HA. Glaucoma. *Lancet*. (2011) 377:1367–77. doi: 10.1016/S0140-6736(10)61423-7
- Armstrong RA. Visual problems associated with traumatic brain injury. *Clin Exp Optom*. (2018) 101:716–26. doi: 10.1111/cxo.12670
- Frick KD, Singman EL. Cost of military eye injury and vision impairment related to traumatic brain injury: 2001–2017. *Mil Med*. (2019) 184:e338–43. doi: 10.1093/milmed/usaa420
- Yin TC, Voorhees JR, Genova RM, Davis KC, Madison AM, Britt JK, et al. Acute axonal degeneration drives development of cognitive, motor, and visual deficits after blast-mediated traumatic brain injury in mice. *eNeuro*. (2016) 3:ENEURO.0220. doi: 10.1523/ENEURO.0220-16.2016
- Medda A, Funk R, Ahuja K, Kamimori G. Measurements of infrasound signatures from grenade blast during training. *Mil Med*. (2021) 186:523–8. doi: 10.1093/milmed/usaa423
- Pang JJ. Roles of the ocular pressure, pressure-sensitive ion channel, and elasticity in pressure-induced retinal diseases. *Neural Regen Res*. (2021) 16:68–72. doi: 10.4103/1673-5374.286953
- Arnadottir J, Chalfie M. Eukaryotic mechanosensitive channels. *Annu Rev Biophys*. (2010) 39:111–37. doi: 10.1146/annurev.biophys.37.032807
- Brohawn SG. How ion channels sense mechanical force: insights from mechanosensitive K2P channels TRAAK, TREK1, and TREK2. *Ann N Y Acad Sci*. (2015) 1352:20–32. doi: 10.1111/nyas.12874
- Cox CD, Bavi N, Martinac B. Origin of the force: the force-from-lipids principle applied to Piezo channels. *Curr Top Membr*. (2017) 79:59–96. doi: 10.1016/bs.ctm.2016.09.001
- Krizaj D, Cordeiro S, Strauß O. Retinal TRP channels: cell-type-specific regulators of retinal homeostasis and multimodal integration. *Prog Retin Eye Res*. (2023) 92:101114. doi: 10.1016/j.preteyeres.2022.101114
- Guarino BD, Paruchuri S, Thodeti CK. The role of TRPV4 channels in ocular function and pathologies. *Exp Eye Res*. (2020) 201:108257. doi: 10.1016/j.exer.2020.108257
- Lorin C, Vogeli I, Niggli E. Dystrophic cardiomyopathy: role of TRPV2 channels in stretch-induced cell damage. *Cardiovasc Res*. (2015) 106:153–62. doi: 10.1093/cvr/cvv021
- Sappington RM, Sidorova T, Long DJ, Calkins DJ. TRPV1: contribution to retinal ganglion cell apoptosis and increased intracellular Ca<sup>2+</sup> with exposure to hydrostatic pressure. *Invest Ophthalmol Vis Sci*. (2009) 50:717–28. doi: 10.1167/iovs.08-2321
- Gao F, Yang Z, Jacoby RA, Wu SM, Pang JJ. The expression and function of TRPV4 channels in primate retinal ganglion cells and bipolar cells. *Cell Death Dis*. (2019) 10:364–1576. doi: 10.1038/s41419-019-1576-3
- Sappington RM, Sidorova T, Ward NJ, Chakravarthy R, Ho KW, Calkins DJ. Activation of transient receptor potential vanilloid-1 (TRPV1) influences how retinal

## Acknowledgments

We thank Dr. Roy Jacoby for project and technical collaboration.

## Conflict of interest

The authors declare that the research was conducted in the absence of any commercial or financial relationships that could be construed as a potential conflict of interest.

## Publisher's note

All claims expressed in this article are solely those of the authors and do not necessarily represent those of their affiliated organizations, or those of the publisher, the editors and the reviewers. Any product that may be evaluated in this article, or claim that may be made by its manufacturer, is not guaranteed or endorsed by the publisher.

ganglion cell neurons respond to pressure-related stress. *Channels*. (2015) 9:102–13. doi: 10.1080/19336950.2015.1009272

17. Ryskamp DA, Witkovsky P, Barabas P, Huang W, Koehler C, Akimov NP, et al. The polymodal ion channel transient receptor potential vanilloid 4 modulates calcium flux, spiking rate, and apoptosis of mouse retinal ganglion cells. *J Neurosci*. (2011) 31:7089–101. doi: 10.1523/JNEUROSCI.0359-11.2011

18. Taylor L, Arner K, Ghosh F. Specific inhibition of TRPV4 enhances retinal ganglion cell survival in adult porcine retinal explants. *Exp Eye Res*. (2016) 154:10–21.

19. Zimov S, Yazulla S. Localization of vanilloid receptor 1 (TRPV1/VR1)-like immunoreactivity in goldfish and zebrafish retinas: restriction to photoreceptor synaptic ribbons. *J Neurocytol*. (2004) 33:441–52. doi: 10.1023/B:NEUR.0000046574.72380.e8

20. Yazulla S, Studholme KM. Vanilloid receptor like 1 (VRL1) immunoreactivity in mammalian retina: colocalization with somatostatin and purinergic P2X1 receptors. *J Comp Neurol*. (2004) 474:407–18. doi: 10.1002/cne.20144

21. Gilliam JC, Wensel TG. TRP channel gene expression in the mouse retina. *Vis Res*. (2011) 51:2440–52. doi: 10.1016/j.visres.2011.10.009

22. Pang JJ, Gao F, Wu SM. Generators of pressure-evoked currents in vertebrate outer retinal neurons. *Cells*. (2021) 10:1288. doi: 10.3390/cells10061288

23. Long Y, Kozhemyakin M, Wu SM, Pang JJ. TRPV4 affects visual signals in photoreceptors and rod bipolar cells. *Front Cell Neurosci*. (2024) 18:1404929. doi: 10.3389/fncel.2024.1404929

24. Xu JW, Slaughter MM. Large-conductance calcium-activated potassium channels facilitate transmitter release in salamander rod synapse. *J Neurosci*. (2005) 25:7660–8. doi: 10.1523/JNEUROSCI.1572-05.2005

25. Pelucchi B, Grimaldi A, Moriondo A. Vertebrate rod photoreceptors express both BK and IK calcium-activated potassium channels, but only BK channels are involved in receptor potential regulation. *J Neurosci Res*. (2008) 86:194–201. doi: 10.1002/jnr.21467

26. Sakaba T, Ishikane H, Tachibana M. Ca<sup>2+</sup>-activated K<sup>+</sup> current at presynaptic terminals of goldfish retinal bipolar cells. *Neurosci Res*. (1997) 27:219–28. doi: 10.1016/S0168-0102(97)01155-3

27. Fink M, Lesage F, Duprat F, Heurteaux C, Reyes R, Fosset M, et al. A neuronal two P domain K<sup>+</sup> channel stimulated by arachidonic acid and polyunsaturated fatty acids. *EMBO J*. (1998) 17:3297–308. doi: 10.1093/emboj/17.12.3297

28. Hughes S, Foster RG, Peirson SN, Hankins MW. Expression and localisation of two-pore domain (K2P) background leak potassium ion channels in the mouse retina. *Sci Rep*. (2017) 7:46085. doi: 10.1038/srep46085

29. Enyedi P, Czizjak G. Molecular background of leak K<sup>+</sup> currents: two-pore domain potassium channels. *Physiol Rev*. (2010) 90:559–605. doi: 10.1152/physrev.00029.2009

30. Maingret F, Patel AJ, Lesage F, Lazdunski M, Honore E. Lysophospholipids open the two-pore domain mechano-gated K<sup>+</sup> channels TREK-1 and TRAAK. *J Biol Chem*. (2000) 275:10128–33. doi: 10.1074/jbc.275.14.10128

31. Patel AJ, Lazdunski M, Honore E. Lipid and mechano-gated 2P domain K<sup>+</sup> channels. *Curr Opin Cell Biol*. (2001) 13:422–8. doi: 10.1016/S0955-0674(00)00231-3

32. Kim Y, Bang H, Gnatenco C, Kim D. Synergistic interaction and the role of C-terminus in the activation of TRAAK K<sup>+</sup> channels by pressure, free fatty acids and alkali. *Pflugers Arch.* (2001) 442:64–72. doi: 10.1007/s004240000496
33. Patel AJ, Honore E, Maingret F, Lesage F, Fink M, Duprat F, et al. A mammalian two pore domain mechano-gated S-like K<sup>+</sup> channel. *EMBO J.* (1998) 17:4283–90. doi: 10.1093/emboj/17.15.4283
34. Lesage F, Terrenoire C, Romey G, Lazdunski M. Human TREK2, a 2P domain mechano-sensitive K<sup>+</sup> channel with multiple regulations by polyunsaturated fatty acids, lysophospholipids, and Gs, Gi, and Gq protein-coupled receptors. *J Biol Chem.* (2000) 275:28398–405. doi: 10.1074/jbc.M002822200
35. Suzuki M, Mizuno A, Kodaira K, Imai M. Impaired pressure sensation in mice lacking TRPV4. *J Biol Chem.* (2003) 278:22664–8. doi: 10.1074/jbc.M302561200
36. Liedtke W, Choe Y, Marti-Renom MA, Bell AM, Denis CS, Sali A, et al. Vanilloid receptor-related osmotically activated channel (VR-OAC), a candidate vertebrate osmoreceptor. *Cell.* (2000) 103:525–35. doi: 10.1016/S0092-8674(00)00143-4
37. Alessandri-Haber N, Yeh JJ, Boyd AE, Parada CA, Chen X, Reichling DB, et al. Hypotonicity induces TRPV4-mediated nociception in rat. *Neuron.* (2003) 39:497–511. doi: 10.1016/S0896-6273(03)00462-8
38. Li W, Feng Z, Sternberg PW, Xu XZ. A *C. elegans* stretch receptor neuron revealed by a mechanosensitive TRP channel homologue. *Nature.* (2006) 440:684–7. doi: 10.1038/nature04538
39. Kang L, Gao J, Schafer WR, Xie Z, Xu XZ. *C. elegans* TRP family protein TRP-4 is a pore-forming subunit of a native mechanotransduction channel. *Neuron.* (2010) 67:381–91. doi: 10.1016/j.neuron.2010.06.032
40. Loukin S, Zhou X, Su Z, Saimi Y, Kung C. Wild-type and brachyolmia-causing mutant TRPV4 channels respond directly to stretch force. *J Biol Chem.* (2010) 285:27176–81. doi: 10.1074/jbc.M110.143370
41. Ciura S, Liedtke W, Bourque CW. Hypertonicity sensing in organum vasculosum lamina terminalis neurons: a mechanical process involving TRPV1 but not TRPV4. *J Neurosci.* (2011) 31:14669–76. doi: 10.1523/JNEUROSCI.1420-11.2011
42. Ryskamp DA, Jo AO, Frye AM, Vazquez-Chona F, Mac Aulay N, Thoreson WB, et al. Swelling and eicosanoid metabolites differentially gate TRPV4 channels in retinal neurons and glia. *J Neurosci.* (2014) 19:15689–700.
43. Liu C, Montell C. Forcing open TRP channels: mechanical gating as a unifying activation mechanism. *Biochem Biophys Res Commun.* (2015) 460:22–5. doi: 10.1016/j.bbrc.2015.02.067
44. McGahon MK, Fernandez JA, Dash DP, McKee J, Simpson DA, Zholos AV, et al. TRPV2 channels contribute to stretch-activated cation currents and myogenic constriction in retinal arterioles. *Invest Ophthalmol Vis Sci.* (2016) 57:5637–47. doi: 10.1167/iovs.16-20279
45. Leonelli M, Martins DO, Britto LR. Retinal cell death induced by TRPV1 activation involves NMDA signaling and upregulation of nitric oxide synthases. *Cell Mol Neurobiol.* (2013) 33:379–92. doi: 10.1007/s10571-012-9904-5
46. Pang JJ. The variety of mechanosensitive ion channels in retinal neurons. *Int J Mol Sci.* (2024) 25:4877. doi: 10.3390/ijms25094877
47. Liu W, Zhang W, Wang C, Song J, Li K, Zhang X, et al. TRPV4 antagonist suppresses retinal ganglion cell apoptosis by regulating the activation of CaMKII and TNF- $\alpha$  expression in a chronic ocular hypertension rat model. *Int Immunopharmacol.* (2024) 130:111811. doi: 10.1016/j.intimp.2024.111811
48. Nilius B, Szallasi A. Transient receptor potential channels as drug targets: from the science of basic research to the art of medicine. *Pharmacol Rev.* (2014) 66:676–814. doi: 10.1124/pr.113.008268
49. Patel N, Pass A, Mason S, Gibson CR, Otto C. Optical coherence tomography analysis of the optic nerve head and surrounding structures in Long-duration international Space Station astronauts. *JAMA Ophthalmol.* (2018) 136:193–200. doi: 10.1001/jamaophthalmol.2017.6226
50. Zhou D, Wei W, Tian B, Wang C, Shi X, Jiao X. Observation and management of retinal changes related to diving in professional divers. *Chin Med J.* (2014) 127:729–33. doi: 10.3760/cma.j.issn.0366-6999.20132620
51. Mowatt L, Foster T. Sphenoidal sinus mucocele presenting with acute visual loss in a scuba diver. *BMJ Case Rep.* (2013) 2013:bcr2013010309. doi: 10.1136/bcr-2013-010309
52. Jiang X, Wang G, Lee AJ, Stornetta RL, Zhu JJ. The organization of two new cortical interneuronal circuits. *Nat Neurosci.* (2013) 16:210–8. doi: 10.1038/nn.3305
53. Wang G, Wyskiel DR, Yang W, Wang Y, Milbern LC, Lalanne T, et al. An optogenetics-and imaging-assisted simultaneous multiple patch-clamp recording system for decoding complex neural circuits. *Nat Protoc.* (2015) 10:397–412. doi: 10.1038/nprot.2015.019
54. Gao F, Maple BR, Wu SM. I4AA-sensitive chloride current contributes to the center light responses of bipolar cells in the tiger salamander retina. *J Neurophysiol.* (2000) 83:3473–82. doi: 10.1152/jn.2000.83.6.3473
55. Pang JJ, Gao F, Lem J, Bramblett DE, Paul DL, Wu SM. Direct rod input to cone BCs and direct cone input to rod BCs challenge the traditional view of mammalian BC circuitry. *Proc Natl Acad Sci U S A.* (2010) 107:395–400. doi: 10.1073/pnas.0907178107
56. Maple BR, Wu SM. Glycinergic synaptic inputs to bipolar cells in the salamander retina. *J Physiol.* (1998) 506:731–44. doi: 10.1111/j.1469-7793.1998.731bv.x
57. Pang JJ, Gao F, Wu SM. Light-evoked excitatory and inhibitory synaptic inputs to ON and OFF alpha ganglion cells in the mouse retina. *J Neurosci.* (2003) 23:6063–73. doi: 10.1523/JNEUROSCI.23-14-06063.2003
58. Pang JJ, Gao F, Wu SM. Segregation and integration of visual channels: layer-by-layer computation of ON-OFF signals by amacrine cell dendrites. *J Neurosci.* (2002) 22:4693–701. doi: 10.1523/JNEUROSCI.22-11-04693.2002
59. Pang JJ, Gao F, Wu SM. Ionotropic glutamate receptors mediate OFF responses in light-adapted ON bipolar cells. *Vis Res.* (2012) 68:48–58. doi: 10.1016/j.visres.2012.07.012
60. Pang JJ, Wu SM. Morphology and immunoreactivity of retrogradely double-labeled ganglion cells in the mouse retina. *Invest Ophthalmol Vis Sci.* (2011) 52:4886–96. doi: 10.1167/iovs.10-5921
61. Pang JJ, Gao F, Wu SM. Light responses and morphology of bNOS-immunoreactive neurons in the mouse retina. *J Comp Neurol.* (2010) 518:2456–74. doi: 10.1002/cne.22347
62. Zhang J, Yang Z, Wu SM. Development of cholinergic amacrine cells is visual activity-dependent in the postnatal mouse retina. *J Comp Neurol.* (2005) 484:331–43. doi: 10.1002/cne.20470
63. Fink M, Duprat F, Lesage F, Reyes R, Romey G, Heurteaux C, et al. Cloning, functional expression and brain localization of a novel unconventional outward rectifier K<sup>+</sup> channel. *EMBO J.* (1996) 15:6854–62. doi: 10.1002/j.1460-2075.1996.tb01077.x
64. Cohen MR, Huynh KW, Cawley D, Moiseenkova-Bell VY. Understanding the cellular function of TRPV2 channel through generation of specific monoclonal antibodies. *PLoS One.* (2013) 8:e85392. doi: 10.1371/journal.pone.0085392
65. Shah KR, Guan X, Yan J. Structural and functional coupling of calcium-activated BK channels and calcium-permeable channels within nanodomain signaling complexes. *Front Physiol.* (2022) 12:796540. doi: 10.3389/fphys.2021.796540
66. Vivas O, Moreno CM, Santana LF, Hille B. Proximal clustering between BK and ca (V)<sub>1.3</sub> channels promotes functional coupling and BK channel activation at low voltage. *Elife.* (2017) 6:e28029. doi: 10.7554/eLife.28029
67. Cerecedo D, Martínez-Vieyra I, Sosa-Peinado A, Cornejo-Garrido J, Ordaz-Pichardo C, Benítez-Cardoza C. Alterations in plasma membrane promote overexpression and increase of sodium influx through epithelial sodium channel in hypertensive platelets. *Biochim Biophys Acta.* (2016) 1858:1891–903. doi: 10.1016/j.bbmem.2016.04.015
68. Ruan YC, Guo JH, Liu X, Zhang R, Tsang LL, Dong JD, et al. Activation of the epithelial Na<sup>+</sup> channel triggers prostaglandin E release and production required for embryo implantation. *Nat Med.* (2012) 18:1112–7. doi: 10.1038/nm.2771
69. Liu HB, Zhang J, Sun YY, Li XY, Jiang S, Liu MY, et al. Dietary salt regulates epithelial sodium channels in rat endothelial cells: adaptation of vasculature to salt. *Br J Pharmacol.* (2015) 172:5634–46. doi: 10.1111/bph.13185
70. Pang JJ, Paul DL, Wu SM. Survey on amacrine cells coupling to retrograde-identified ganglion cells in the mouse retina. *Invest Ophthalmol Vis Sci.* (2013) 54:5151–62. doi: 10.1167/iovs.13-11774
71. Pang JJ, Yang Z, Jacoby RA, Wu SM. Cone synapses in mammalian retinal rod bipolar cells. *J Comp Neurol.* (2018) 526:1896–909. doi: 10.1002/cne.24456
72. Pasteels B, Rogers J, Blachier F, Pochet R. Calbindin and calretinin localization in retina from different species. *Vis Neurosci.* (1990) 5:1–16. doi: 10.1017/S0952523800000031
73. Fischer AJ, Foster S, Scott MA, Sherwood P. Transient expression of LIM-domain transcription factors is coincident with delayed maturation of photoreceptors in the chicken retina. *J Comp Neurol.* (2008) 506:584–603. doi: 10.1002/cne.21578
74. Zhang H, Cuenca N, Ivanova T, Church-Kopish J, Frederick JM, Macleish PR, et al. Identification and light-dependent translocation of a cone-specific antigen, cone arrestin, recognized by monoclonal antibody 7G6. *Invest Ophthalmol Vis Sci.* (2003) 44:2858–67. doi: 10.1167/iovs.03-0072
75. Zhang J, Yang Z, Wu SM. Immunocytochemical analysis of spatial organization of photoreceptors and amacrine and ganglion cells in the tiger salamander retina. *Vis Neurosci.* (2004) 21:157–66. doi: 10.1017/S0952523804042075
76. Pow DV, Wright LL, Vaney DI. The immunocytochemical detection of amino-acid neurotransmitters in paraformaldehyde-fixed tissues. *J Neurosci Methods.* (1995) 56:115–23. doi: 10.1016/0165-0270(94)00113-U
77. Pang JJ, Gao F, Wu SM. Light responses and amacrine cell modulation of morphologically-identified retinal ganglion cells in the mouse retina. *Vis Res.* (2023) 205:108187. doi: 10.1016/j.visres.2023.108187
78. Raman IM, Bean BP. Resurgent sodium current and action potential formation in dissociated cerebellar Purkinje neurons. *J Neurosci.* (1997) 17:4517–26. doi: 10.1523/JNEUROSCI.17-12-04517.1997
79. Fohlmeister JF, Cohen ED, Newman EA. Mechanisms and distribution of ion channels in retinal ganglion cells: using temperature as an independent variable. *J Neurophysiol.* (2010) 103:1357–74. doi: 10.1152/jn.00123.2009
80. Chatterjee S, Vyas R, Chalamalasetti SV, Sahu ID, Clatot J, Wan X, et al. The voltage-gated sodium channel pore exhibits conformational flexibility during slow inactivation. *J Gen Physiol.* (2018) 150:1333–47. doi: 10.1085/jgp.201812118

81. Zhou Z, Martinac B. Mechanisms of PIEZO Channel inactivation. *Int J Mol Sci.* (2023) 24:14113. doi: 10.3390/ijms241814113
82. Wang L, Shi KP, Li H, Huang H, Wu WB, Cai CS, et al. Activation of the TRAAK two-pore domain potassium channels in rd 1 mice protects photoreceptor cells from apoptosis. *Int J Ophthalmol.* (2019) 12:1243–9. doi: 10.18240/ijo.2019.08.03
83. Zhang XT, Xu Z, Shi KP, Guo DL, Li H, Wang L, et al. Elevated expression of TREK-TRAAK K (2P) channels in the retina of adult rd 1 mice. *Int J Ophthalmol.* (2019) 12:924–9. doi: 10.18240/ijo.2019.06.07
84. Hardie RC. Photosensitive TRPs. *Handb Exp Pharmacol.* (2014) 223:795–826. doi: 10.1007/978-3-319-05161-1\_4
85. He D, Pan Q, Chen Z, Sun C, Zhang P, Mao A, et al. Treatment of hypertension by increasing impaired endothelial TRPV4-KCa2.3 interaction. *EMBO Mol Med.* (2017) 9:1491–503. doi: 10.15252/emmm.201707725
86. Dryn DO, Melnyk MI, Melanaphy D, Kizub IV, Johnson CD, Zholos AV. Bidirectional TRP/L type ca (2+) channel/RyR/BK (ca) molecular and functional signalplex in vascular smooth muscles. *Biomol Ther.* (2023) 13:759. doi: 10.3390/biom13050759
87. Liu L, Guo M, Lv X, Wang Z, Yang J, Li Y, et al. Role of transient receptor potential vanilloid 4 in vascular function. *Front Mol Biosci.* (2021) 8:677661. doi: 10.3389/fmolb.2021.677661
88. Weitlauf C, Ward NJ, Lambert WS, Sidorova TN, Ho KW, Sappington RM, et al. Short-term increases in transient receptor potential vanilloid-1 mediate stress-induced enhancement of neuronal excitation. *J Neurosci.* (2014) 34:15369–81. doi: 10.1523/JNEUROSCI.3424-14.2014
89. Saito T, Kondo H, Toyoda JI. Ionic mechanisms of two types of on-center bipolar cells in the carp retina. I. The responses to central illumination. *J Gen Physiol.* (1979) 73:73–90. doi: 10.1085/jgp.73.1.73
90. Kaneko A, Tachibana M. A voltage-clamp analysis of membrane currents in solitary bipolar cells dissociated from *Carassius auratus*. *J Physiol.* (1985) 358:131–52. doi: 10.1113/jphysiol.1985.sp015544
91. Szmajda BA, DeVries SH. Glutamate spillover between mammalian cone photoreceptors. *J Neurosci.* (2011) 31:13431–41. doi: 10.1523/JNEUROSCI.2105-11.2011
92. Wu SM. Synaptic transmission from rods to bipolar cells in the tiger salamander retina. *Proc Natl Acad Sci U S A.* (1985) 82:3944–7.
93. Cho AK, Sampath AP, Weiland JD. Physiological response of mouse retinal ganglion cells to electrical stimulation: effect of soma size. *Ann Int Conf IEEE Eng Med Biol Soc.* (2011) 2011:1081–4. doi: 10.1109/IEMBS.2011.6090252
94. Lakk M, Young D, Baumann JM, Jo AO, Hu H, Krizaj D. Polymodal TRPV1 and TRPV4 sensors Colocalize but do not functionally interact in a subpopulation of mouse retinal ganglion cells. *Front Cell Neurosci.* (2018) 12:353. doi: 10.3389/fncel.2018.00353
95. Attwell D, Laughlin SB. An energy budget for signaling in the grey matter of the brain. *J Cereb Blood Flow Metab.* (2001) 21:1133–45. doi: 10.1097/00004647-200110000-00001
96. Ulbricht W. Sodium channel inactivation: molecular determinants and modulation. *Physiol Rev.* (2005) 85:1271–301. doi: 10.1152/physrev.00024.2004
97. Minke B. Light-induced reduction in excitation efficiency in the trp mutant of *Drosophila*. *J Gen Physiol.* (1982) 79:361–85. doi: 10.1085/jgp.79.3.361